PCCP

Direct imaging of Electric field behavior in 2,7-Diphenyl[1]benzothieno[3,2-b][1]benzothiophene Organic Field-Effect transistors by Sum-Frequency Generation Imaging Microscopy

Journal:	*Physical Chemistry Chemical Physics*
Manuscript ID	CP-ART-12-2020-006407.R2
Article Type:	Paper
Date Submitted by the Author:	04-Feb-2021

Complete List of Authors:	Katagiri, Chiho; National Institute of Advanced Industrial Science and Technology Tsukuba Center Tsukuba Central Miyamae, Takayuki; Chiba University, Graduate School of Engineering; Molecular Chirality Research Center, Chiba University Li, Hao; University of Houston, Department of Chemistry Yang, Fangyuan ; University of Houston, Department of Chemistry Baldelli, Steven; University of Houston, Department of Chemistry

ARTICLE

Direct imaging of Electric field behavior in 2,7-Diphenyl[1]benzothieno[3,2-b][1]benzothiophene Organic Field-Effect transistors by Sum-Frequency Generation Imaging Microscopy

Received 00th January 20xx,
Accepted 00th January 20xx

DOI: 10.1039/x0xx00000x

Chiho Katagiri,[a] Takayuki Miyamae,[*,b,c] Hao Li, Fangyuan Yang[d] and Steven Baldelli[*,d]

Sum-frequency generation imaging microscopy combined with compressive-sensing (CS-SFG) is a powerful micro-spectroscopic technique for probing interfaces and surfaces with a spatial resolution where contrast is based on the chemical functional groups. We reported the use of CS-SFG technique to probe the electric field due to charge accumulation and internal electric field in operating organic field-effect transistors (OFETs) with aluminum oxide and octadecylphosphonic acid (ODPA) self-assembled monolayer as the gate dielectric layer, and 2,7-diphenyl[1]benzothieno[3,2-b][1]benzothiophene (DPh-BTBT) as the semiconductor layer. In addition, the electric field behavior was discussed by difference in the electric field induced SFG intensity between open-circuit and the voltage application condition. The SFG peak of CH stretching mode derived from methyl groups of ODPA and phenyl groups of DPh-BTBT could be observed at each interface of ODPA/DPh-BTBT or DPh-BTBT/Au, respectively. Moreover, the electric field induced SFG coming from the ODPA/DPh-BTBT show the presence of intense electric field due to charge injection and accumulation near the drain and source electrode edges under the operation of OFETs. Our studies show that the electric field-induced SFG imaging technique is useful for probing the local electric field distribution or charge accumulation behavior in OFETs under operating conditions.

Introduction

The organic field-effect transistors (OFETs) with the flexibility and low-cost processability have widely attracted much attention as the key component of “plastic” electronics devices, such as flexible displays, radio-frequency identification tags and sensor devices [1]–[3]. Hence, the stability of OFETs under the ambient conditions has become more and more important, thus the air-stable thienoacene-based organic semiconductors have been developed [4], [5]. Recently, the OFET performance was remarkably improved owing to the development of thienoacene-based semiconductors with various substituents and the optimization of the crystal structure of organic semiconductors and the device fabrication techniques. Although the current field-effect mobility in OFETs reaches comparable to that of amorphous silicon transistors, a further improvement in the mobility of OFETs is required to enable practical use of innovative organic electronics devices.

Since, in the case of OFETs, the injected charge carriers are accumulated and transported at the dielectric/semiconductor interface under the application of voltage, the important issue is to investigate the spatial charge distribution and the accumulation behavior at the dielectric/semiconductor interface. An understanding of the interface phenomenon in OFETs and the development of tools for probing specific interfaces is essential to further improve the OFET performance. Although the charge distribution at the interface has been studied by measuring the surface potential using Kelvin probe microscopy [6] and atomic force microscopy potentiometry [7], the direct observation of charge distribution and any microscopic information is difficult at a specified interface. In particular, under the operation of OFETs, the investigation of charging behavior is a challenging subject at the dielectric interface covered in the semiconductor layer.

[a] *Nanomaterials Research Institute, National Institute of Advanced Industrial Science and Technology (AIST), 1-1-1 Higashi, Tsukuba, Ibaraki 305-8565, Japan.*
[b] *Graduate School of Engineering, Chiba University, 1-33 Yayoi-cho, Inage-ku, Chiba 263-8522, Japan.*
[c] *Molecular Chirality Research Center, Chiba University, 1-33 Yayoi-cho, Inage-ku, Chiba, 263-8522, Japan.*
[d] *Department of Chemistry, University of Houston, Houston, Texas 77204-5003, United States.*
† Electronic Supplementary Information (ESI) available. See
DOI: 10.1039/x0xx00000x

Second-order nonlinear optical spectroscopies are powerful techniques for investigating the charging behavior at the specific interfaces of OFETs. Iwamoto and co-workers have pioneered in the use of electric field induced second harmonic generation (EFI-SHG) to probe the dielectric-field formed by the charge accumulation at the dielectric/semiconductor interface [8], [9]. Some papers reported that the electric field induced sum-frequency generation (EFI-SFG) can probe the behavior of charge accumulation of OFETs and succeeded in probing the enhancement of SFG signals derived from the gate dielectric materials and the non-resonant background due to the charge accumulation [13]–[15]. When the static electric field E_0 is applied to the system, the SFG signal intensity (I_{SFG}) is given by [11]

$$I_{SFG} \propto |P|^2 = |\chi^{(2)} + \chi^{(3)}E_0|^2 I_{VIS}(\omega) I_{IR}(\omega) \#(1)$$

where P is the nonlinear polarization, I_{VIS} (ω) and I_{IR} (ω) are the intensities of the visible (VIS) and infrared (IR) light source, respectively. $\chi^{(2)}$ and $\chi^{(3)}$ are the second- and third-order nonlinear susceptibilities, and E_0 is the magnitude of the DC electric field. The effective nonlinear susceptibility contains the electric field terms, and the effective SFG field amplitude is proportional to E_0. Therefore, the SFG intensity can be used to investigate the electric field distribution under the operation of OFETs. In addition, since the SFG spectroscopy is available to probe the vibrational states of interfacial molecules, it is very sensitive to the interfaces within complicated structure devices with multiple organic semiconductor films. Thus, the EFI-SFG spectroscopy has been used to observe the charge accumulation behavior at the interfaces within devices such as organic light-emitting diodes in recent years [10]–[12].

This work aims to directly observe and visualize the electric field due to charge transportation and accumulation under the operation of OFETs with 2,7-diphenyl[1]benzothieno[3,2-b][1]benzothiophene (DPh-BTBT) by using sum-frequency generation imaging microscopy coupled with compressive sensing technique (CS-SFG). SFG imaging microscopy is an exciting novel micro-spectroscopic technique for measuring both dimensional and spatial position information on molecules existing at the surface and interfaces with high spatial and spectral resolutions [16]–[18]. This compressive sensing technique combined with SFG imaging has great potential to solve the low speed of data acquisition issues as compared with the conventional mapping method [19]. We used the CS-SFG technique for investigating the changes of electric field distribution, and reported the results of monitoring the SFG images as well as the spectra of both the channel and electrode region of OFETs. The images reflecting the SFG signals of C-H stretching mode derived from methyl groups of ODPA and phenyl groups of DPh-BTBT were clearly observed at each interface of ODPA/DPh-BTBT or DPh-BTBT/Au. Moreover, the electric field behavior under the operation of OFETs was discussed by investigating the difference in electric field induced SFG intensity between the open-circuit condition and the voltage application condition.

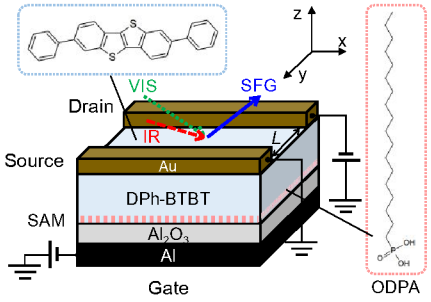

Figure 1. Schematic representation of the top-contact/bottom-gate OFET device.

Experimental

Figure 1 shows the schematic illustration of the top-contact bottom-gate structure of the OFET device employed in this work. First, 30 nm thick aluminum (Al, Nilaco Co., 99.999 %) was deposited by vacuum thermal evaporation on a glass substrate as the gate electrode. The gate dielectric consists of a 10 nm thick aluminum oxide (Al_2O_3) layer and a self-assembled monolayer (SAM) of octadecylphosphonic acid (ODPA, Tokyo Chemical Industry Co. Ltd). The aluminum oxide was formed by the anodic oxidation of the Al layer using a 10 mM water solution of citric acid (Wako Pure Chemical Co.) at a DC voltage of 5 V [20]. The ODPA was prepared by dipping the Al/Al_2O_3 substrate in a 5mM isopropanol (Wako Chemical Industry Co. Ltd) solution of ODPA [21]. The DPh-BTBT (Sigma-Aldrich, sublimated grade, 99%) of 50 nm thick was deposited by vacuum thermal evaporation on the gate dielectric layer. Finally, 50 nm thick gold (Au, Nilaco Co., 99.99 %) was deposited on the DPh-BTBT layer as the drain (D) and source (S) electrodes through a shadow mask. Au electrodes were patterned to produce two different channel lengths with L = 50 μm and 300 μm, and channel width with W = 2.0 mm. The devices of larger channel sizes (L = 300 μm) were used for SFG experiments. We confirmed the operation of the OFET device with L = 50 μm and L = 300 μm as shown in supplemental Figs. S1 and S2. Electrical characterization was performed using Agilent B2902A source-measure unit. The hole mobility in the OFET device with DPh-BTBT was estimated to be 0.22 cm^2/Vs (L = 50 μm). The OFET performance is the same as that of the previous paper [5].

The optical system of CS-SFG imaging microscopy employed herein was described in these papers [16, 22]. For the CS-SFG system, a Yb:KGW laser (Pharos, LIGHT CONVERSION) was used to generate the picosecond visible (VIS) pulses of wavelength 515 nm and the femtosecond infrared (IR) pulses with gaussian shape. The VIS and IR pulses were irradiated to the OFET surface with incident angles of 45° and 70°, respectively. Since the overlapped beam area of the visible and IR laser pulses (ca. 700 μm diameter) were larger than the channel length of the OFET device (300 μm), the SFG signals originates from both the channel region and the drain/source electrodes region. The spatial resolution of the current CS-SFG system is approximately 10 μm [18]. The SFG spectra and SFG imaging data were collected in SSP (s-polarized SF signal, s-

polarized visible beam, and p-polarized infrared beam) and PPP polarization combinations. For both SFG measurements, the measurement configuration was illustrated in Fig. 1, and the incidence plane was perpendicular to the channel length direction (Fig. 1, x-z plane). In this experiment, the spectra and imaging data were not normalized by the intensity of IR and VIS beams.

Results and Discussion

Figure 2 shows the SFG spectra obtained from the OFET device under different applied gate-source voltage (V_{gs}) or drain-source voltage (V_{ds}). The intensity of the sum frequency output is given by the equation as follows:

$$I(\omega_{SF}) \propto \left| \chi_{NR} e^{i\varphi} + \sum_q \frac{A_q}{\omega_{IR} - \omega_q + i\Gamma_q} \right|^2 \#(2)$$

where χ_{NR} and ϕ is the nonresonant contribution to the nonlinear susceptibility and the phase difference between resonant and nonresonant term, ω_{IR} and ω_{VIS} are the frequencies of the IR beam and the VIS, respectively. A_q, ω_q, and Γ_q are respectively the amplitude, resonant frequency, and damping coefficient of vibrational mode q. The SFG peak at 3064 cm^{-1} was assigned to the C-H stretching modes of the phenyl termini in the DPh-BTBT molecules [23], [24]. The peaks at around 2880 and 2940 cm^{-1} were attributed to the symmetric (s) and Fermi resonance (FR) C-H stretching modes of methyl groups (CH_3), respectively [24]. The broad feature ranging from 2900 to 3000 cm^{-1} arise from the IR beams with Gaussian shape centered at around 2980 cm^{-1}, as shown in the PPP-polarized spectra of supplemental material Fig. S3. These peaks originated from the terminal alkyl chains of ODPA covered by the DPh-BTBT layer because the ODPA on Al_2O_3 used as the gate dielectric is the only molecule containing CH_3 group. In the aliphatic C-H stretching region, no methylene (CH_2) peaks were observed under the open circuit condition, indicating that the alkyl chains of ODPA have well-ordered all-trans conformation even after the deposition of DPh-BTBT. When applying V_{gs} voltage or both V_{gs} and V_{ds} voltage, the

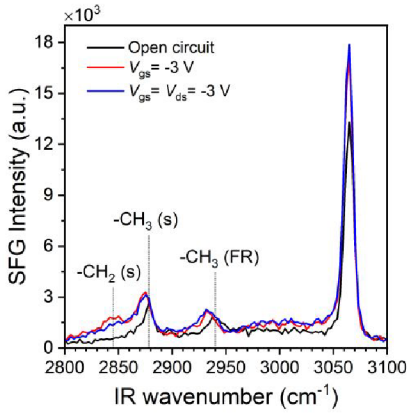

Figure 2. SSP polarized SFG spectra of the OFET device under different voltage conditions.

intensities of all SFG peaks derived from the phenyl and methyl groups and non-resonant SFG signals increased as compared to the intensities from the open circuit condition. The increases in the SFG signal intensities were due to the electric field enhancement caused by the accumulated charge carriers at the ODPA/DPh-BTBT interface [13], [25], [26]. Furthermore, the peaks at around 2880 and 2940 cm^{-1} slightly red-shifted under the application of the voltages. A shift of vibrational frequency is considered to be due to the change in the phase term ϕ of non-resonant susceptibility in Eq. (2) due to the increase in the non-resonant amplitude under the application of voltages [13]. Interestingly, the peak at 2847 cm^{-1} originates from the symmetric stretching mode of CH_2 appeared by applying the V_{gs} voltage, which was not observed in the ODPA film under the open circuit condition. Such spectral changes by applying strong electric field have been also observed in the previous SFG studies of OFETs by Ye and co-workers [14]. One may think that the peak appearance of the CH_2 is presumed to be due to the formation of gauche defects in the alkyl chain of ODPA molecules by applying the gate voltage. When V_{gs} is applied to the OFET, in the normal direction in the channel region of the thin gate dielectric (Al_2O_3/ODPA) will have an electric field strength of the order of 10^6 V/cm caused by the accumulated charges. Since the electric field induced effect caused by the charge accumulation at the organic interface is the results of the second and third-order nonlinear susceptibility, the latter of which is not interface specific and is observed in the thin boundary layer as thick as the space charge accumulated at the interface region. Thus, one would

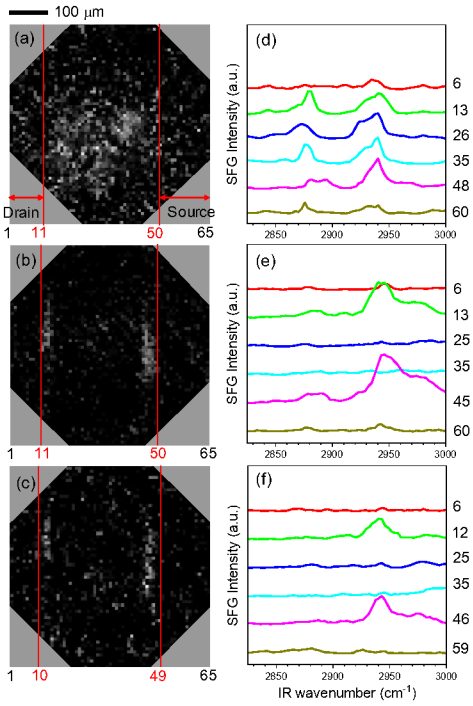

Figure 3. SSP-polarized SFG images reflecting the peak originated from CH_3 (FR) of ODPA (2940 cm^{-1}) for (a) open circuit condition, (b) V_{gs} = −3 V and (c) V_{gs} = V_{ds} = −3 V. The numbers from 1 to 65 show the position of a rectangular area 1 ×27 pixels. SFG spectra at each position for (d) open circuit condition, (e) V_{gs} = −3 V for and (f) V_{gs} = V_{ds} = −3 V. The peak intensities at 2870 cm^{-1} are weaker in (e) and (f) than that in (d) because the center wavenumber of the IR pulse is different from that in (d).

expect that $\chi^{(2)}$-symmetry forbidden methylene vibrations

would appear due to partial $\chi^{(3)}$-symmetry of the signal contribution when an electric field is present.

To discuss the electric field behavior in OFET under operating conditions, the images of SSP polarized SFG signal distributions were obtained by using the CS-SFG technique. Figures 3 (a-c) are reconstructed images from the slice of the SFG signal frequency (2940 cm^{-1}) attributed to the CH_3 (FR) for different applied V_{gs} or V_{ds} voltages. It is difficult to observe simultaneously the spectra originated from CH_3 (s) and phenyl CH, because the bandwidth of IR laser for CS-SFG measurement is 120 cm^{-1} [18]. Hence, we focused on the methyl resonance CH_3 (FR) to determine the electric field behavior. Figures 3 (d-f) show the SFG spectra at the wavenumber of 2800-3000 cm^{-1} for some measuring positions. Each of SFG spectra were extracted with a rectangular area 1 $\times$ 27 pixels, and the six positions were selected from No. 1 to 65 (Fig. S4). In this experiment, the incident IR wavenumber or beam intensity, were optimized for each condition. For open circuit condition (before the application voltage) as shown in Fig. 3 (d), the SFG spectra were acquired with the IR centered at 2912 cm^{-1}. For the application of V_{gs} and/or V_{ds} voltage, it was centered at 2950 cm^{-1} (Figs. 3 (e) and (f)).

As shown in Figs. 3 (a) and (d), the SFG images and signals originated from CH_3 (FR) for open circuit condition were almost uniformly distributed in the whole channel region. This result indicates that the orientation of the ODPA is uniform on the Al_2O_3 surface within the collection area. The detailed intensity distribution of the SFG signal obtained across the channel from drain to source electrode is shown in supplemental Fig. S5. Upon applying the V_{gs} voltage, however, the SFG signal of CH_3 (FR) at located around 30-40 μm from the Au electrode edges becomes stronger than that at the center of the channel region (Fig. 3 (b)). Figure 3 (e) clearly shows that the peak originated from CH_3 (FR) were observed in the vicinity of the Au electrode edges (position Nos. 13 and 45) to the channel region, indicating that the stronger electric fields than that of the middle of the channel region (Nos. 25 and 35) were generated at the ODPA/DPh-BTBT interface close to the edges of both Au electrodes. Since the change in the intensity of the Fermi resonance peak due to the application of bias is small as shown in Fig. 2, it is difficult to judge from the contrast in Fig. 3 that there is a clear enhancement in the channel region or not. On the other hand, the intensity of the PPP-polarized SFG signal of CH_3 (FR) is almost uniformly distributed inside the channel region by applying the V_{gs} voltage (Fig. S6). Similar behavior is also reported by the electronic SFG imaging microscopy of OFET by Nakai and co-workers [25]. According to the device simulation of the OFETs, it has been reported that the charge injection is taking place from near the electrode edge of source or drain due to the electric fields of the vertical (z-direction) and along the channel length direction (y-direction), and then the charge accumulation occurs within the first few layers at the dielectric/semiconductor interface [27]. In this experiment, since the holes injected from both Au electrodes are accumulated in the channel region at the ODPA/DPh-BTBT interface, the electric field generated by the accumulated charges should have a component in the normal direction under applying the V_{gs} voltage. For the SSP polarization combination, the third-order susceptibility tensor component of yyzz is permitted under applying the V_{gs} voltage because the electric field generated by the accumulated charges has a component in the surface normal direction [28, 29]. Furthermore, although the tensor component of yyzy is primarily forbidden for an isotropic medium [29], the yyzy component is also allowed due to the anisotropy induced by the y-direction electric fields which induce the charge injection from near the electrode edge and the charge accumulation at the ODPA/DPh-BTBT interface. Thus, the intense SFG signal of CH_3 (FR) from the ODPA/DPh-BTBT interface was observed mostly due to in-plane E field close to the Au electrodes. In case of the PPP-polarized image, unlike the case of the SSP, it is reasonable to consider that it reflects the electric field strength in the normal direction because the zzzz tensor component is associated with the PPP polarization combination. Therefore, the PPP-polarized SFG signal of CH_3 (FR) from the ODPA/DPh-BTBT interface was observed uniformly in the whole channel region.

When applying both V_{gs} and V_{ds} voltage of −3 V (saturation region), a similar phenomenon to the case of Fig. 3 (b) was observed as shown in Fig. 3 (c). In this condition, it is recognized that the accumulated holes located at the ODPA/DPh-BTBT interface at the source electrode side is generating a high vertical field [15], and the holes are extracted by the high horizontal electric field in depletion region near the drain electrode side. It seems reasonable that the existence of the bright region in the reconstructed image near the source electrode side is due to the accumulation of injected holes. In the case of the drain electrode side, however, the accumulated holes were depleted at the drain electrode side under the application of V_{gs} and V_{ds} voltage. This phenomenon is the well-known pinch-off effect. Since the potential difference between the gate electrode and the channel near the drain electrode disappears with the increase in V_{ds}, a charge carrier depletion region is formed near the drain electrode, and then the injected holes are extracted by the high electric field in depletion region. Thus, the SFG signal region near the edge of the drain electrode is considered to be induced by the electric field due to the depletion region [30]. Although the reconstructed images and the intensity distribution look very similar for V_{gs} = −3 V and V_{gs} = V_{ds} = −3 V (Figs. S5 (b) and (c)), the peak shapes of CH_3 (FR) near the drain side (No. 12) and the source side (No. 46) seem to be different shapes with respect to those under the V_{gs} = V_{ds} = −3 V (Fig. 3 (f)). The shape of the SFG near the electrodes are almost the same when only V_{gs} = −3 V is applied (Nos. 13 and 45) (Fig. 3 (e)). It seems natural that the difference in spectral shapes between that near electrodes is attributed to the difference in the electric field source. The origin of this electric field is considered to be different between the electric field generated by the accumulated charges (at both S and D) under application of V_{gs} voltage only, and the electric field formed under by the depletion layer under the application of both V_{gs} and V_{ds} voltages (vertical field due to accumulation at S and horizontal field due to depletion at D).

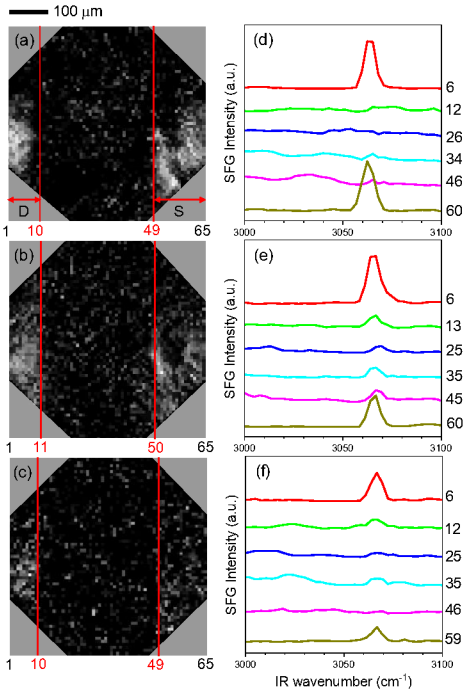

Figure 4. SSP-polarized SFG images reflecting the peak originated from phenyl group of DPh-BTBT (3065 cm^{-1}) for (a) open circuit condition, (b) V_{gs} = −3 V and (c) V_{gs} = V_{ds} = −3 V. SFG spectra of (d) open circuit condition, (e) V_{gs} = −3 V for and (f) V_{gs} = V_{ds} = −3 V. The dark spot at the center of the source electrode shown in the SFG images is the scratch of the Au electrode.

The reconstructed images of the peak frequency (3065 cm^{-1}) attributed to phenyl CH stretching of the phenyl group in DPh-BTBT for different applied V_{gs} and/or V_{ds} voltages as shown in Figs. 4 (a)-(c). The SFG images were acquired with the IR centered at 2992 cm^{-1} or 2950 cm^{-1} for open circuit condition (after the application voltage) or applied voltage, respectively. Interestingly, the bright region of the images accord with Au electrode region, indicating that the relative intensity of SFG signals at the Au electrode regions is stronger than it at the channel regions. The relatively strong peak at Au region was clearly observed in Figs. 4 (d)-(f). The Au films with a thickness of 50 nm show a good electric conductivity, and the Au deposited by vacuum evaporation on the DPh-BTBT film was used as the source and drain electrodes. When the Au thickness is from 40 to 60 nm, it has been reported that the observation of the phenyl CH stretching mode under the Au electrode was due to the strong electromagnetic field associated with the surface plasmon polariton and the collective electron resonance as in the case of the surface-enhanced Raman scattering [31]. Thus, we concluded that the SFG signals at the Au electrode region were attributed to phenyl CH stretching originated from DPh-BTBT/Au interface, not from ODPA/DPh-BTBT interface.

The SFG signals at channel region were provided by the ODPA/DPh-BTBT and DPh-BTBT/air interface. As shown in Fig. 4 (d), for open circuit condition, the relative peak intensities at the channel region were much weaker than it at Au region. In contrast, for the application of V_{gs} and V_{ds} voltage, Figs. 4 (e) and (f) show that the relative intensity of the signals at the channel region increased compared to it at the Au region. The increase in the relative intensity of the phenyl CH stretch at the channel region results from the electric field induced effect caused by the charge accumulation at the ODPA/DPh-BTBT interface. In addition, the result show that the signals at the channel region were attributed to phenyl CH stretching originated from ODPA/DPh-BTBT interface, not from DPh-BTBT/air interface.

Here, we observed the interesting features in the difference in SFG contrast of phenyl CH between drain and source electrodes interface (DPh-BTBT/Au). For open circuit condition, the relative SFG intensity between drain and source electrodes region was similar as shown in Figs. 4 (a) and (d). In the similar way, for the application of V_{gs} = −3 V, the relative intensity between drain and source electrode region did not change (Figs. 4 (b) and (e)). In contrast, for V_{gs} = V_{ds} = −3 V (Figs. 4 (c) and (f)), the SFG intensity at the drain electrode region (spectra of No. 6) was stronger as compared with that at the source electrode (spectra of No. 59). The significant difference was shown in the results of SFG intensity profiles (Fig. S7). The difference in SFG contrast between the source and drain electrodes are considered to be caused by the difference in the strength of internal electric field at DPh-BTBT/Au interface. The depletion layer due to the Schottky barrier is formed for open circuit, thus an internal electric field was induced at both drain and source electrode interface (DPh-BTBT/Au). When applying V_{gs} = −3 V, the barrier was reduced at both drain and source interface. The relative strength of electric fields was similar for both electrode interface. Although for V_{gs} = V_{ds} = −3 V the electric field strength in the depletion layer decrease under the source electrode interface, it increases at drain electrode interface under negative voltage application. Since the electric field strength modified the SFG intensity of phenyl CH stretching mode under Au electrode associated with the surface plasmon resonance, the difference in the SFG contrast between the drain and source electrodes must be caused by the change of the internal electric field in depletion layer at the DPh-BTBT/Au interface.

Conclusions

In this work, we reported the use of sum-frequency generation imaging microscopy using a compressive sensing technique (CS-SFG) for investigation of the local electric field behavior under the operation of OFET devices. Changes in the SFG intensities derived from the methyl CH stretching of ODPA and the phenyl CH stretching of DPh-BTBT were observed for different applied the V_{gs} and V_{ds} voltages, which result from the electric-field induced effect. The reconstructed CS-SFG images and the intensity distribution of SFG signals across the channel region upon applying V_{gs} = −3 V show the presence of intense electric field due to charge injection and accumulation at the ODPA/DPh-BTBT interface near Au electrode edges. When applying V_{gs} = V_{ds} = −3 V, different contrast between the drain and source electrode region was revealed, which might be due to the formation of the internal electric field due to Schottky barrier at the DPh-BTBT/Au interface of the drain

electrode side, while such the electric field decrease in the source electrode side. The results indicated that the CS-SFG imaging technique can be expanded to investigate the behavior of charge accumulation, charge transportation and the visualization of the electric field during operation of the OFET devices. Therefore, this chemical imaging technique is expected to bring new perspectives for the characterization of the organic field-effect transistors.

Conflicts of interest

There are no conflicts to declare.

Acknowledgements

This paper is based on results obtained from a project commissioned by the New Energy and Industry Technology Development Organization (NEDO) (P16010). The author would like to thank Prof. A. Morita (Tohoku Univ.) for constructive discussion. SB would like to acknowledge the WM Keck Foundation and NSF (CHE-1610453) for funding of the CS-SFG microscope.

Notes and references

1 H. Matsui, Y. Takeda and S. Tokito, Flexible and Printed Organic Transistors: from Materials to Integrated Circuits, *Organic Electronics*, 2019, **75**, 105432.

2 A. Yamamura, H. Matsui, M. Uno, N. Isahaya, Y. Tanaka, M. Kudo, M. Ito, C. Mitsui, T. Okamoto and J. Takeya, Painting Integrated Complementary Logic Circuits for Single-Crystal Organic Transistors: A Demonstration of a Digital Wireless Communication Sensing Tag, *Adv. Electron. Mater.,* 2017, **3**, 1–6.

3 S. G. Surya, H. N. Raval, R. Ahmad, P. Sonar, K. N. Salama and V. R. Rao, Organic field effect transistors (OFETs) in environmental sensing and health monitoring, A review. *TrAC - Trends in Analytical Chemistry,* 2019, **111**, 27–36.

4 K. Takimiya, S. Shinamura, I. Osaka and E. Miyazaki, Thienoacene-based organic semiconductors, *Adv. Mater.,* 2011, **23**, 4347–4370.

5 K. Takimiya, H. Ebata, K. Sakamoto, T. Izawa, T. Otsubo and Y. Kunugi, 2,7-Diphenyl[1]benzothieno[3,2-b]benzothiophene, a new organic semiconductor for air-stable organic field-effect transistors with mobilities up to 2.0 $cm^2 V^{-1} s^{-1}$, *J. Am. Chem. Soc,* 2006, **128**, 12604–12605.

6 Y. Hu, V. Pecunia, L. Jiang, C. A. Di, X. Gao and H. Sirringhaus, Scanning Kelvin Probe Microscopy Investigation of the Role of Minority Carriers on the Switching Characteristics of Organic Field-Effect Transistors, *Adv. Mater.,* 2016, **28**, 4713–4719.

7 M. Nakamura, N. Goto, N. Ohashi, M. Sakai and K. Kudo, Potential mapping of pentacene thin-film transistors using purely electric atomic-force-microscope potentiometry, *Appl. Phys., Lett.* 2005, **86**, 1–3.

8 T. Manaka, E. Lim, R. Tamura, D. Yamada and M. Iwamoto, Probing of the electric field distribution in organic field effect transistor channel by microscopic second-harmonic generation, *Appl. Phys. Lett.,* 2006, **89**, 1–4.

9 T. Manaka, F. Liu, M. Weis and M. Iwamoto, Diffusionlike electric-field migration in the channel of organic field-effect transistors, *Phys. Rev. B,* 2008, **78**, 1–4.

10 T. Sato, T. Miyamae, H. Ohata and T. Tsutsui, Direct observations of the charge behavior of a high-efficiency blue organic light-emitting diode under operating conditions using electric-field-induced doubly resonant sum-frequency-generation vibrational spectroscopy, *Org. Electron.,* 2019, **74**, 118–125.

11 T. Miyamae, N. Takada and T. Tsutsui, Probing buried organic layers in organic light-emitting diodes under operation by electric-field-induced doubly resonant sum-frequency generation spectroscopy, *Appl. Phys. Lett.,* 2012, **101**, 1–5.

12 T. Miyamae, N. Takada, H. Ohata and T. Tsutsui, Direct probing of charge carrier behavior in multilayered organic light-emitting diode devices by time-resolved electric-field-induced sum-frequency generation spectroscopy, *Appl. Phys. Express,* 2017, **10**, 1–4.

13 T. C. Anglin, D. B. O'Brien and A. M. Massari, Monitoring the Charge Accumulation Process in Polymeric Field-Effect Transistors via in Situ Sum Frequency Generation Timothy, *J. Phys. Chem.,* 2010, **114**, 17629–17637.

14 H. Ye, J. Huang, J. R. Park, H, E. Katz and D. H. Gracias, Correlations between SFG spectra and electrical properties of organic field effect transistors, *J. Phys. Chem. C,* 2007, **111**, 13250–13255.

15 S. G. Motti, L. S. Cardoso, D. J. C. Gomes, Faria and P. B. Miranda, Probing Device Degradation and Electric Fields in Polymeric Field-Effect Transistors by SFG Vibrational Spectroscopy, *J. Phys. Chem. C,* 2018, **122**, 10450–10458.

16 D. Zheng, L. Lu, Y. Li, K. F. Kelly and S. Baldelli, Compressive Broad-Band Hyperspectral Sum Frequency Generation Microscopy to Study Functionalized Surfaces, *J. Phys. Chem. Lett.,* 2016, **7**, 1781–1787.

17 Z. Sun, D. Zheng and S. Baldelli, Study of the Wetting of Paraffin Films on the Metal Surface in the Dynamic Dip-Coating Process Using Compressive-Sensing Sum-Frequency Generation Microscopy, *J. Phys. Chem. C,* 2018, **122**, 26543–26553.

18 D. Zheng, L. Lu, K. F. Kelly and S. Baldelli, Chemical Imaging of Self-Assembled Monolayers on Copper Using Compressive Hyperspectral Sum Frequency Generation Microscopy, *J. Phys. Chem. B,* 2018, **122**, 464–471.

19 X. Cai, B. Hu, T. Sun and K. F. Kelly and S. Baldelli, Sum frequency generation-compressive sensing microscope, *J. Chem. Phys.,* 2011, **135**, 19.

20 M. Kaltenbrunner, P. Stadler, R. Schwodiauer, A. W. Hassel, N. S. Sariciftci and S. Bauer, Anodized aluminum oxide thin films for room-temperature-processed, flexible, low-voltage organic non-volatile memory elements with excellent charge retention, *Adv. Mater.,* 2011, **23**, 4892–4896.

21 H. Klauk, U. Zschieschang, J. Pflaum and M. Halik, Ultralow-power organic complementary circuits, *Nature,* 2007, **445**, 745–748.

22 H. Li, K. F. Kelly and S. Baldelli, *J. Chem. Phys.*, 2020, **153**, 19091.

23 M. Oh-e, S. C. Hong and Y. R. Shen, Orientations of phenyl sidegroups and liquid crystal molecules on a rubbed polystyrene surface, *Appl. Phys. Lett.,* 2002, **80**, 784–786.

24 S. R. Walter, J. Youn, J. D. Emery, S. Kewalramani, J. W. Hennek, M. J. Bedzyk, A. Facchetti, T. J. Marks and F. M. Geiger, In-situ probe of gate dielectric-semiconductor interfacial order in organic transistors: Origin and control of large performance sensitivities, *J. Am. Chem. Soc.,* 2012, **134**, 11726–11733.

25 I. F. Nakai, M. Tachioka, A. Ugawa, T. Ueda, K. Watanabe and Y. Matsumoto, Molecular structure and carrier distributions at semiconductor/dielectric interfaces in organic field-effect transistors studied with sum frequency generation microscopy, *Appl. Phys. Lett.,* 2009, **95**, 1–4.

26 T. C. Anglin, Z. Sohrabpour and A. M. Massari, Nonlinear spectroscopic markers of structural change during charge accumulation in organic field-effect transistors, *J. Phys. Chem. C,* 2011, **115**, 20258–20266.
27 C. H. Shim, T. Sekiya, and R. Hattori, Device simulation of ditch and elevated electrode structures in organic thin-film transistors, *Jpn. J. Appl. Phys.,* 2012, **51**, 024303.
28 T. Joutsuka, T. Hirano, M. Sprik and A. Morita, Effects of third-order susceptibility in sum frequency generation spectra: a molecular dynamics study in liquid water, *Phys. Chem. Chem. Phys*., 2018, ***20***, 3040–3053.
29 R. W. Boyd, *Nonlinear Optics,* 3rd ed., Academic Press: London, 2008.
30 G. D. Tournadre, F. Reisdorffer, R. Rödel, O. Simonetti, H. Klauk and L. Giraudet, High voltage surface potential measurements in ambient conditions: Application to organic thin-film transistor injection and transport characterization, *J. Appl. Phys.,* 2016, **119**, 125501.
31 Y. Shen, S. Nihonyanagi, K. Fujishima and K. Uosaki, Conformational Order of Octadecanethiol (ODT) Monolayer at Gold/Solution Interface: Internal Reflection Sum Frequency Generation (SFG) Study, *Stud. Surf. Sci. Catal.,* 2001, **132**, 705–710.